AGRICULTURAL AND FOREST METEOROLOGY XXX (2008) XXX–XXX

available at www.sciencedirect.com

ScienceDirect

journal homepage: www.elsevier.com/locate/agrformet

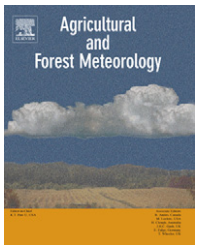

Modeling radiation and photosynthesis of a heterogeneous savanna woodland landscape with a hierarchy of model complexities

Qi Chen [a,*], Dennis Baldocchi [b], Peng Gong [b,c], Todd Dawson [b]

[a] Department of Geography, University of Hawai'i at Manoa, 422 Saunders Hall, 2424 Maile Way, Honolulu, HI 96822, USA
[b] Department of Environmental Science, Policy, and Management, 137 Mulford Hall, University of California at Berkeley, Berkeley, CA 94720, USA
[c] The State Key Lab of Remote Sensing Science, Postal Box 9718, Beijing 100101, PR China[1]

ARTICLE INFO

Article history:
Received 26 July 2007
Received in revised form
23 January 2008
Accepted 24 January 2008

Keywords:
Clumping
Markov
Poisson
Heterogeneity
Photosynthesis
Phytoactinometry

ABSTRACT

Simple but realistic modeling of radiation transfer within heterogeneous canopy has been a challenging research question for decades and is critical for predicting ecological processes such as photosynthesis. The Markov model proposed by [Nilson, T., 1971. A theoretical analysis of the frequency of gaps in plant stands. Agric. Meteorol. 8, 25–38] is theoretically sound to meet this challenge. However, it has not been widely used because of the difficulty of determining the clumping factor. We propose an analytical approach to calculate clumping factors based on the average characteristics of vegetation distributed across a landscape. In a savanna woodland in California, we simulate the photosynthesis of the landscape in three different ways: (1) the crown envelope and location of each tree is spatially explicitly specified, (2) the canopy is assumed to be horizontally homogeneous within which leaves are randomly dispersed as a Poisson process, and (3) the canopy is horizontally homogeneous but leaves are clumped and distributed with a Markov process. We find that the Markov model can achieve much better performance than the Poisson model by incorporating the crown-level clumping. The results indicate that our approach of calculating clumping factors has applications in terrestrial ecosystem modeling, particularly where accurate representation of "system heterogeneity" (e.g., savannas and woodlands) is required.

1. Introduction

Savannas, inhabited by one-fifth of the world's human population, are one of the Earth's most important heterogeneous terrestrial biomes (Ramankutty and Foley, 1999). Since savannas are anticipated to be among the ecosystems that are most sensitive to future land use and climate changes (Bond et al., 2003; Sankaran et al., 2005), it is important to gain a mechanistic understanding of their vegetation–atmosphere exchange. Processed-based ecological models are one approach for achieving this understanding. However, modeling savanna ecosystems is very challenging because savannas are typically characterized with sparsely distributed individual trees, both horizontally and vertically heterogeneous.

Since solar radiation is a controlling driver of many ecological processes, one of the major challenge is to model

* *Corresponding author*. Tel.: +1 510 717 9839; fax: +1 808 3512.
E-mail address: qichen@hawaii.edu (Q. Chen).

[1] Jointly sponsored by Institute of Remote Sensing Applications, Chinese Academy of Sciences, and Beijing Normal University.

0168-1923/$ – see front matter
doi:10.1016/j.agrformet.2008.01.020

radiation interception realistically for heterogeneous landscapes like savannas. A three-dimensional individual-tree based model can be used to characterize the canopy morphology details as much as possible (Charles-Edwards and Thorpe, 1976; Allen, 1974). However, at broad spatial scales simpler models, which assume a homogeneous canopy (such as big-leaf models), are preferred because of the demanding computation and parameterization requirements of individual-tree based models (Sinclair et al., 1976). When the simpler models are used, it is essential to know the answers to two key questions. First, when compared to an individual-tree based model, what are the errors of radiation modeling due to the simplification of canopies? Second, how can we improve the simple models so that they can achieve comparable performance to individual-tree based models?

For the first question, previous studies have investigated the effects of canopy simplification on radiation interception for heterogeneous canopies (Asrar et al., 1992; Jarvis and Leverenz, 1983; Norman and Welles, 1983; Andrieu and Sinoquet, 1993). For example, Asrar et al. (1992) simulated canopies with different leaf area index and canopy cover within a plot of 50 m by 50 m and compared the 1D and 3D models. They found that the 1D approach results in an overestimation of both canopy reflectivity and PAR absorptivity as compared to a 3D calculation. The discrepancy is especially large at lower canopy leaf area indices and generally decreases with increasing leaf area. Their analysis indicated that the leaf area index of a canopy is less of an instructive parameter than ground cover and clump leaf area index for modeling radiation within these canopies. Norman and Welles (1983) tested a three-dimensional general array model in a crop canopy in and compared it with a big-leaf model. They found that at a leaf area index of four, the general ellipsoidal array model predicts the same direct beam PAR intercepted as the random model on a daily basis. However, at leaf area indices of 0.5, 1.0, and 2.0 the random model overestimates daily intercepted PAR by 25, 17, and 7%, respectively. Another finding is that the sunfleck fraction is most affected by clumping foliage at intermediate leaf area indexes when adjacent rows are just beginning to approach closure. Andrieu and Sinoquet (1993) compared a two-dimensional model (one dimension in vertical direction, the other is one horizontal direction) and a big-leaf model in predicting the gap fraction of an artificial row canopy. It was found that the big-leaf model significantly underestimated the gap fraction and overestimated the light interception.

To make 1D models to simulate comparable canopy optical properties (such as canopy reflectance, transmittance, and interception) as more detailed 3D models, previous research has used either used look-up table methods (Pinty et al., 2004) or used non-Poisson models to characterize the non-randomness of canopy. Two of such computationally efficient models exist: the binomial model (Monteith, 1965; De Wit, 1965) and the Markov model (Nilson, 1971). Baldocchi et al. (1985) used a negative binomial distribution to describe the foliage clumping and obtained an improved simulation of direct radiation within canopy than the Poisson distribution. Baldocchi and Harley (1995), to our best knowledge, first demonstrated the importance of clumping in modeling photosynthesis of natural ecosystems by comparing computations with direct eddy flux measurements of CO_2 exchange. However, compared to the binomial models, the Markov model is more general (Nilson, 1971) and widely used (Norman and Welles, 1983; Andrieu and Sinoquet, 1993; Kucharik et al., 1999; Baldocchi et al., 1999; Chen et al., 2005). For example, Jonckheere et al. (2006) compared three light extinction models including Poisson, Markov, and negative binomial models; they found that the Markov model was shown to be an appropriate model for LAI inversion from hemispherical photographs in a wide variety of virtual forest stands. Another interesting research work in this field was done by Nilson (1999), who proposed new formulas to calculate gap fraction due to canopy clustering at different structural levels. These formulas also consider the effects of different spatial patterns of trees (including Poisson and binomial distribution) and crown shape on gap fraction.

By incorporating the clumping factor, the Markov model can generate the same light penetration probability P (or gap fraction) or interception probability I as field measurements or simulated results from complex three-dimensional radiation transfer models.

$$P = e^{-k\Omega L} \tag{1}$$

$$I = 1 - e^{-k\Omega L} \tag{2}$$

where L is the leaf area index, k is the extinction coefficient, and Ω is the clumping factor. The key for applying this approach is to calculate the clumping factor given a heterogeneous landscape. Some studies have attempted to find the variables that affect clumping factors and proposed some equations for quantifying clumping factors. For example, Norman and Welles (1983) derived the clumping factor by assuming that the Markov model can intercept the same amount of radiation as the individual-tree model. They found that the clumping factor varied with zenith angle and leaf area index. Andrieu and Sinoquet (1993) derived the clumping factor with a similar approach, however, using the constraint of the same gap fraction. It was also found that the clumping factor depends on zenith angle. Kucharik et al. (1999) calculated clumping factors based on Monte Carlo simulation, but their method is still heuristic and semi-empirical. Chen et al. (2005) for the first time mapped the global-scale clumping index using remotely sensed multi-angular POLDER data assisted by a geometrical optical model. However, the clumping factors are calculated indirectly from remotely sensed signals instead of directly from the characteristics of landscape itself. So far, we still lack a solid understanding on (1) what the deterministic variables for clumping factors are, and (2) how the clumping factors vary with these variables. With no doubt, these questions can be better answered with an analytical instead of empirical approach.

Note that if the Markov model can produce the same gap fraction or interception probability as an individual-tree based model, it also implies that it can produce the same sunlit leaf area index L_{sunlit}. This is evident in the equation of calculating L_{sunlit}:

$$L_{sunlit} = \frac{1 - e^{-k\Omega L}}{k} \tag{3}$$

Please cite this article in press as: Chen, Q. et al., Modeling radiation and photosynthesis of a heterogeneous savanna woodland landscape with a hierarchy of model complexities, Agric. Forest Meteorol. (2008), doi:10.1016/j.agrformet.2008.01.020

In this study, we present an analytical approach to derive clumping factors for heterogeneous canopies based on the constraint that it can produce the same sunlit leaf area index. We use sunlit leaf area index as a constraint because it can help our derivation to intuitively link to physical meanings. In our approach, the clumping factor is dependent on (i) tree spacing to crown width ratio, (ii) crown depth to crown width ratio, (iii) local leaf area index for canopy only, (iv) G-function value, and (v) solar zenith angle.

To test this approach, we use a three-dimensional canopy radiation and photosynthesis model called MAESTRA to construct the canopy inhabiting a savanna woodland in California in three different ways: (1) the shapes and locations of individual trees are explicitly specified; within individual-tree envelopes leaves are randomly distributed, (2) the canopy is simplified as a box within which leaves are randomly distributed, and (3) the canopy is simplified as a box within which leaves are clumped; the clumping factors are calculated with our approach. We then explore how photosynthesis differs among the three scenarios. The modeled photosynthesis is also compared with the CO_2 flux measured by an eddy-covariance tower over the study site.

2. An analytical approach for calculating clumping factors

2.1. Theoretical derivation

To facilitate the calculation of sunlit leaf area index, the landscape is simplified as a mosaic of bare ground and trees,

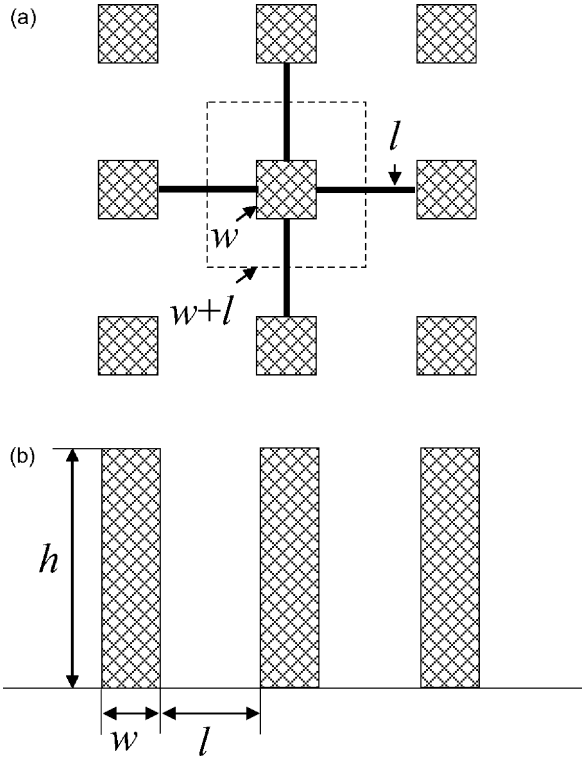

Fig. 1 – The configuration of a heterogeneous landscape. (a and b) are the planar and vertical views of the landscape.

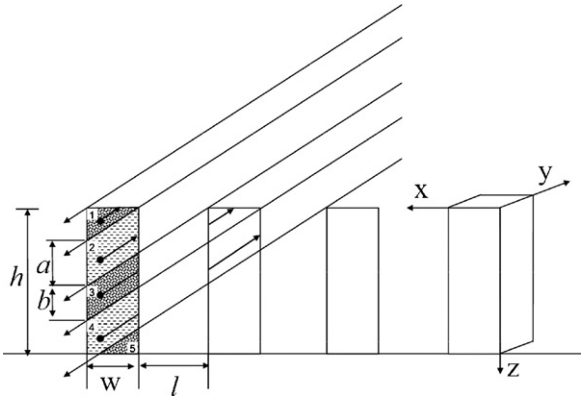

Fig. 2 – Calculation of sunlit leaf area index for heterogeneous landscapes. 1–5 are the index for subvolumes. The long arrows represent the direction of sunlight. *h*, *w*, and *l* are crown depth, crown width, and tree spacing, respectively. *a* and *b* are the parameters used to calculate top and low limits in Eqs. (10) and (11).

where the trees are regularly distributed (Fig. 1a). All trees have the same size and box shapes. The crown width, crown height, and tree spacing are denoted as w, h and l, respectively (Fig. 1b).

For any elementary volume $dv = dx\,dy\,dz$ within the crown, the sunlit leaf area, dA_{sunlit}, can be calculated by:

$$dA_{sunlit} = \rho P_{sunlit}(x, y, z)\,dx\,dy\,dz \tag{5}$$

where ρ is the leaf area volume density in m^2/m^3, which is assumed to be constant over the canopy, $P_{sunlit}(x, y, z)$ is the sunlit leaf area probability within the elementary volume, which can be written as:

$$P_{sunlit}(x, y, z) = e^{-\rho G(\theta) s_{x,y,z}} \tag{6}$$

where $s_{x,y,z}$ is the within-canopy distance of light penetrating to the point (x,y,z) and $G(\theta)$ is the mean projection of unit leaf area along the sunlight direction θ (Ross, 1981). By assuming a turbid media within the envelope of each tree crown, the sunlit leaf area of the tree, denoted as A_{sunlit}, can be calculated by integrating Eq. (5) over the tree volume V.

$$A_{sunlit} = \iiint_{v \in V} \rho P_{sunlit}\,dv = \rho \iiint_{v \in V} e^{-\rho G(\theta) s_{x,y,z}}\,dv \tag{7}$$

For simplicity, let us assume that sunlight is parallel to one side of the box; we also define a coordinate system as follows: the origin is the upper corner that is closer to the sun, the x-axis is parallel to the sunlight and positive along the sunlight direction, the y-axis is perpendicular to the sunlight, and the z-axis is positive downward (Fig. 2). Then, we know

$$\begin{aligned} A_{sunlit} = {} & \rho \int_{x=0}^{w} \int_{y=0}^{w} \int_{z=0}^{h} e^{-\rho G(\theta) s_{x,y,z}}\,dx\,dy\,dz \\ & \rho w \int_{x=0}^{w} \int_{z=0}^{h} e^{-\rho G(\theta) s_{x,z}}\,dx\,dz \end{aligned} \tag{8}$$

To calculate the integral in Eq. (8), we break the tree volume V into subvolumes V_i (i is the index of subvolume and $i = 1, \ldots,$

n) as shown in Fig. 2. The sunlit leaf area of the tree is obtained by integrating the sunlit leaf area for each subvolume separately and then summing them up.

$$A_{sunlit} = \rho w \sum_{i=1}^{n} \int_{x=0}^{w} \int_{z=z_b^i}^{z_t^i} e^{-\rho G(\theta) s_{x,z}^i} \, dx \, dz \tag{9}$$

The reason for doing this is that $s_{x,z}$ can be explicitly expressed for each subvolume. For example, for V_1 in Fig. 2, $s_{x,z}$ is $z/\cos\theta$; for V_2, $s_{x,z}$ is $x/\sin\theta$. More generally,

$$s_{x,z}^i = \begin{cases} \dfrac{z}{\cos\theta} - \dfrac{(i-1)l}{2\sin\theta}, & \text{when } i \text{ is odd} \\ \dfrac{x}{\sin\theta} + \dfrac{(i-2)w}{2\sin\theta}, & \text{when } i \text{ is even} \end{cases} \tag{10}$$

Also, z_t^i and z_b^i can be explicitly expressed as follows:

$$z_t^i = \begin{cases} 0, \quad \text{when } i = 1 \\ \min\left(\dfrac{x}{\sin\theta} + \dfrac{i-1}{2}a + \dfrac{i-3}{2}b, h\right), & \text{when } i \text{ is odd and } i \geq 3 \\ \min\left(\dfrac{x}{\sin\theta} + \dfrac{i-2}{2}a + \dfrac{i-2}{2}b, h\right), & \text{when } i \text{ is even} \end{cases} \tag{11}$$

$$z_b^i = \begin{cases} \min\left(\dfrac{x}{\sin\theta} + \dfrac{i-1}{2}a + \dfrac{i-1}{2}b, h\right), & \text{when } i \text{ is odd} \\ \min\left(\dfrac{x}{\sin\theta} + \dfrac{i}{2}a + \dfrac{i-2}{2}b, h\right), & \text{when } i \text{ is even} \end{cases} \tag{12}$$

where $a = l\cot\theta$, $b = w\cot\theta$.

As shown in Fig. 1(a), the sunlit leaf area index L_{sunlit} over the landscape can be calculated as:

$$L_{sunlit} = \frac{A_{sunlit}}{(w+l)^2} \tag{13}$$

Combine Eqs. (9) and (13), we know that:

$$L_{sunlit} = \frac{\rho/w \sum_{i=1}^{n} \int_{x=0}^{w} \int_{z=z_b^i}^{z_t^i} e^{-\rho G(\theta) s_{x,z}^i} \, dx \, dz}{(1 + l/w)^2} \tag{14}$$

The total leaf area index L over the landscape is:

$$L = \frac{\rho h w^2}{(w+l)^2} = \frac{\rho h}{(1 + l/w)^2} \tag{15}$$

Substitute Eqs. (14) and (15) to (3), and we can calculate the clumping factor. We call these equations the *general* equations for calculating clumping factors. Based on these equations, we know that the calculation of clumping factor requires six parameters: (i) leaf area volume density ρ, (ii) crown depth h, (iii) tree spacing l, (iv) crown width w, (v) solar zenith angle θ, and (vi) G-function value.

2.2. A normalized version of the equations

Next, we will develop another set of equations that all of the tree dimensions are normalized with the crown width, which are called the *normalized* equations for calculating clumping factors. First, let us define new variables x', z', l', and h' so that:

$$x = wx' \tag{16}$$

$$z = wz' \tag{17}$$

$$l = wl' \tag{18}$$

$$h = wh' \tag{19}$$

where l' and h' are the tree spacing to crown width ratio and crown depth to crown width ratio, respectively.

Then, Eq. (14) becomes

$$L_{sunlit} = \frac{\rho w \sum_{i=1}^{n} \int_{x'=0}^{1} \int_{z'=z_b'i}^{z_t'i} e^{-\rho G(\theta) s_{x',z'}^i} \, dx' \, dz'}{(1+l')^2}, \tag{20}$$

and

$$s_{x',z'}^i = \begin{cases} w\left(\dfrac{z'}{\cos\theta} - \dfrac{(i-1)l'}{2\sin\theta}\right), & \text{when } i \text{ is odd} \\ w\left(\dfrac{x'}{\sin\theta} + \dfrac{i-2}{2\sin\theta}\right), & \text{when } i \text{ is even} \end{cases} \tag{21}$$

We also know that the local leaf area index L_{local}, which is the leaf area index only for vegetated area, can be calculated as follows:

$$L_{local} = \rho h \tag{22}$$

Combine Eqs. (20)–(22), and we know that:

$$L_{sunlit} = \frac{(L_{local}/h') \sum_{i=1}^{n} \int_{x'=0}^{1} \int_{z'=z_b'i}^{z_t'i} e^{-(L_{local}/h') G(\theta) s_{x',z'}^i} \, dx' \, dz'}{(1+l')^2} \tag{23}$$

where,

$$s_{x',z'}^i = \begin{cases} \dfrac{z'}{\cos\theta} - \dfrac{(i-1)l'}{2\sin\theta}, & \text{when } i \text{ is odd} \\ \dfrac{x'}{\sin\theta} + \dfrac{i-2}{2\sin\theta}, & \text{when } i \text{ is even} \end{cases} \tag{24}$$

$$z_t'i = \begin{cases} 0, \quad \text{when } i = 1 \\ \min\left(\dfrac{x'}{\sin\theta} + \dfrac{i-1}{2}a' + \dfrac{i-3}{2}b', h'\right), & \text{when } i \text{ is odd and } i >= 3 \\ \min\left(\dfrac{x'}{\sin\theta} + \dfrac{i-2}{2}a' + \dfrac{i-2}{2}b', h'\right), & \text{when } i \text{ is even} \end{cases} \tag{25}$$

$$z_b'i = \begin{cases} \min\left(\dfrac{x'}{\sin\theta} + \dfrac{i-1}{2}a' + \dfrac{i-1}{2}b', h'\right), & \text{when } i \text{ is odd} \\ \min\left(\dfrac{x'}{\sin\theta} + \dfrac{i}{2}a' + \dfrac{i-2}{2}b', h'\right), & \text{when } i \text{ is even} \end{cases}, \tag{26}$$

Table 1 – Base values and ranges for parameters used in the general equations

Parameter	Description	Base value (unit)	Range
h	Crown depth	10 (m)	(0–50)
l	Tree spacing	2 (m)	(0–50)
w	Crown width	2 (m)	(0–50)
ρ	Leaf area volume density	0.2 (m^2/m^3)	(0–1)
G	G-function value	0.5	(0–1)
θ	Solar zenith angle	45 (°)	(0–90)

and $a' = l'\cot\theta$, $b' = \cot\theta$.

Combine Eqs. (15), (18), and (22), and we know that:

$$L = \frac{L_{local}}{(1+l')^2} \quad (27)$$

Eqs. (23) and (27) are mathematically the same as Eqs. (14) and (15), respectively. However, now the input parameters for calculating clumping factors become: (i) local leaf area index for the canopy L_{local}, (ii) crown depth to crown width ratio h', (iii) tree spacing to crown width ratio l', (iv) solar zenith angle θ, and (v) G-function value. The advantage of using this set of equations is that, instead of using leaf area volume density, Eqs. (23) and (27) are dependent on the local leaf area index L_{local}, which is a variable that is widely used (Sellers et al., 1996) and more commonly measured in the field than leaf area volume density (Gower et al., 1999; Jonckheere et al., 2004).

2.3. *Dependence of clumping factors on input parameters*

2.3.1. *The general equations*

To investigate the dependence of clumping factors on the input variables in the *general* equations, we set up a set of base values and their ranges for all of the input parameters (see Table 1). Each time we change one of the parameters and fix the others (Fig. 3). When tree spacing l is zero, the clumping factor is 1 because the canopy is just like a big-leaf. As l increases, the clumping factor drops quickly at the very

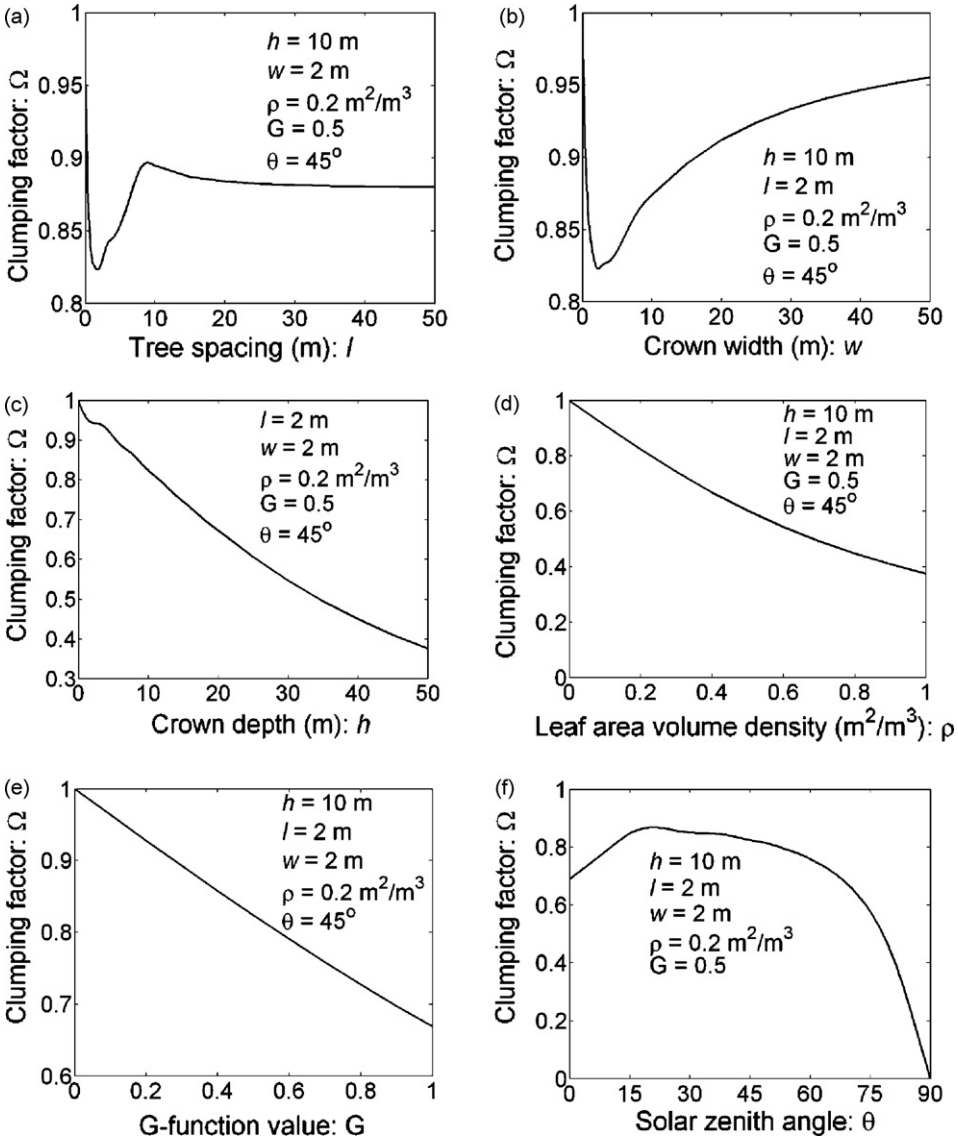

Fig. 3 – Dependence of clumping factors on the input parameters based on the general equations.

Table 2 – Base values and ranges for parameters used in the normalized equations

Parameter	Description	Base value (unit)	Range
h'	Crown depth to crown width ratio	5	(0–25)
l'	Tree spacing to crown width ratio	1	(0–25)
L_{local}	Local leaf area index for canopy	2 (m^2/m^2)	(0–10)
G	G-function value	0.5	(0–1)
θ	Solar zenith angle	45 (°)	(0–90)

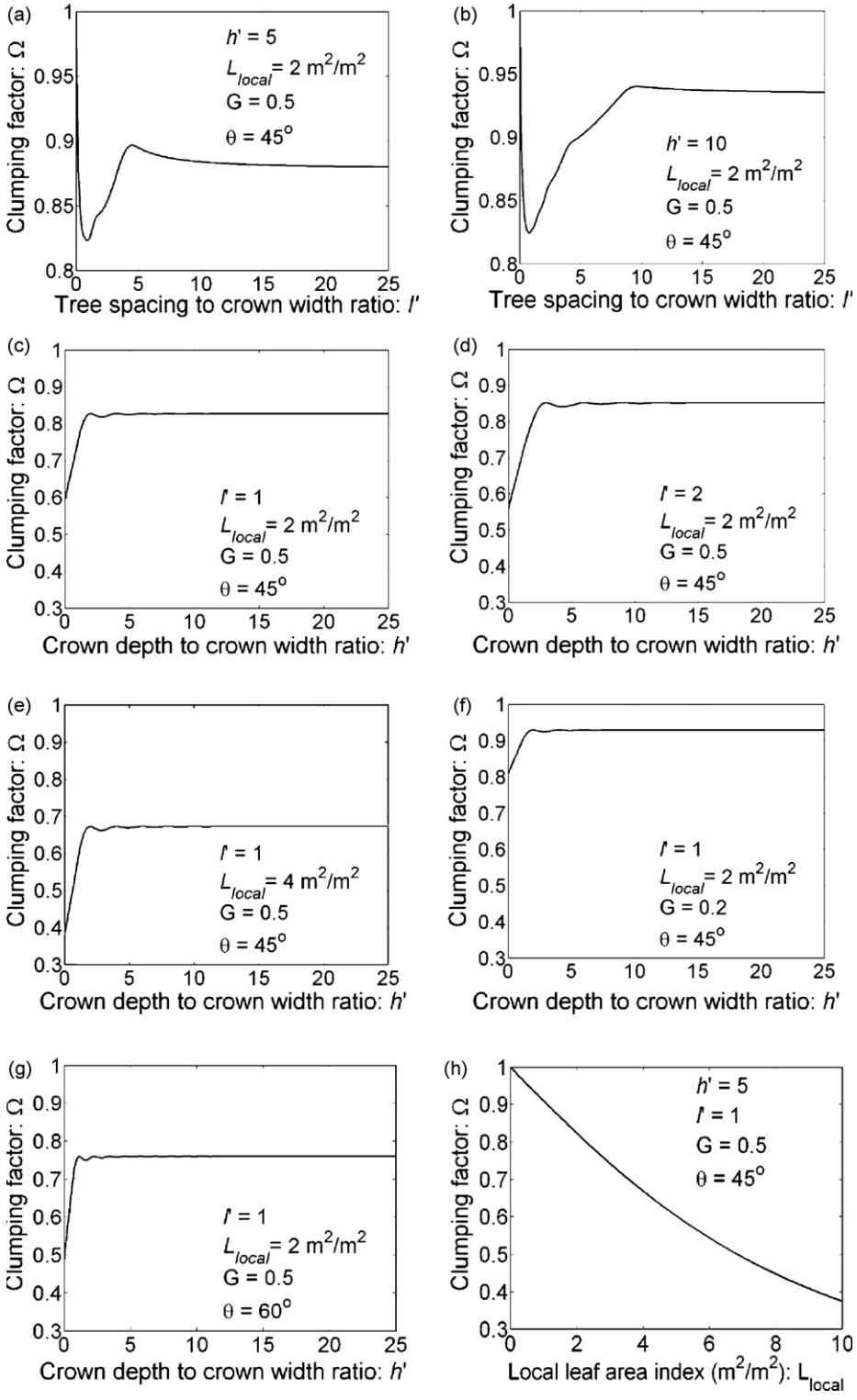

Fig. 4 – Dependence of clumping factors on the input parameters based on the normalized equations.

Please cite this article in press as: Chen, Q. et al., Modeling radiation and photosynthesis of a heterogeneous savanna woodland landscape with a hierarchy of model complexities, Agric. Forest Meteorol. (2008), doi:10.1016/j.agrformet.2008.01.020

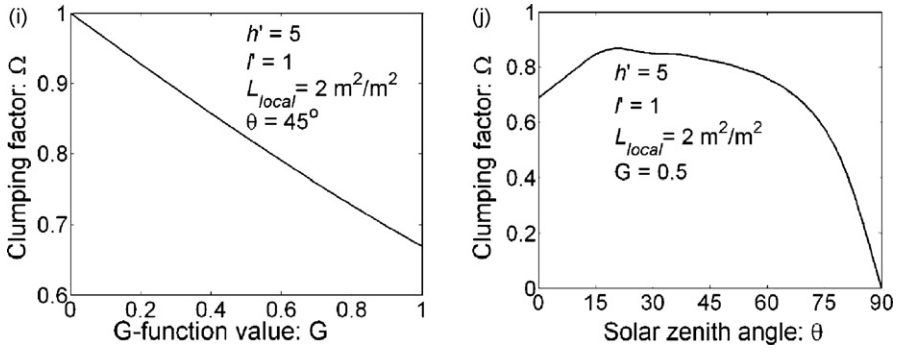

Fig. 4. (Continued).

beginning, followed by an increase and then a decrease again; after certain spacing (>20 m), clumping factors become stable (Fig. 3a). The clumping factor decreases quickly from 1 to smaller values as crown width w increases from 0 to some small value, followed by a steady increase of clumping factor thereafter. The steady increase is consistent with the fact that the canopy looks like a big-leaf as the crown width w increases to a very large value given a small tree spacing (2 m in this case) (Fig. 3b). The clumping factor decreases with crown depth h, leaf area volume density ρ, and G-function value (Fig. 3c–e). When ρ is small, the clumping factor is close to 1. The clumping factor has no monotonic relationship with solar zenith angle. In Fig. 3(f), the clumping factor first increases with solar zenith angle, reaches a maximum around 10°, and then decreases to 0 when the solar zenith angle is 90°. This is interesting because it implies that this particular canopy looks mostly random when the solar zenith angle is some value between 0 and 90°.

2.3.2. *The normalized equations*

The base values and ranges of the parameters in the *normalized* equations (see Table 2) are the corresponding values in Table 1. For example, the base value for local leaf area index is 2 m^2/m^2 according to Eq. (22). The relationship between clumping factors and tree spacing to crown width ratio (Fig. 4a) has the same pattern as the one between clumping factors and tree spacing (Fig. 3a). It is not surprising that clumping factors have the same relationships with G-functions (Figs. 3e and 4i) and solar zenith angle (Figs. 3f and 4j). Due to the close relationship between leaf area volume density and local leaf area index, the relationship between clumping factors and local leaf area index (Fig. 4h) is the same as the one between clumping factors and leaf area volume density (Fig. 3d). However, the relationship between clumping factors and crown depth to crown width ratio (Fig. 4c) shows much difference when compared to the one between clumping factors and crown depth (Fig. 3c). This is because changing the crown depth to crown width ratio h' essentially changes both crown depth and leaf area volume density. Given the same local leaf area index, the increase of h' implies the decrease of leaf area volume density, which means clumping factors will increase (see Fig. 3d). Also, we know the increase of crown depth causes clumping factors to decrease (Fig. 3c). These two opposite trends make clumping factors insensitive to the variations of crown depth to crown width ratio after a certain value. The shape of the curve in Fig. 4c) is very similar to some classical variograms (Chen and Gong, 2004). Four additional curves are derived by changing the base values of crown depth to crown width ratio c (Fig. 4d), the local leaf area index (Fig. 4e), the G-function value (Fig. 4f), and the solar zenith angle (Fig. 4g), it seems that they all have the variogram-like patterns.

Our analytical approach provides a powerful tool to calculate clumping factors given the input parameters and explore the relationships between them. Also, our approach can be used to test the results presented in previous literature. For example, Asrar et al. (1992) concluded that local leaf area index is a very useful parameter for modeling radiation for heterogeneous landscapes. Our results confirm such a conclusion. Moreover, our analysis indicates that other parameters are important too. For instance, Fig. 4(a and b) have the same local leaf area index but different crown depth to crown width ratio h', and the relationship between clumping factors and tree spacing to crown width ratio l' has different patterns.

3. The three-dimensional canopy radiation and photosynthesis model—MAESTRA

We choose an individual-tree based model called MAESTRA (Medlyn, 2004) to test our approach and compare different canopy parameterization and radiative transfer schemes. In the past three decades, a number of spatially explicit 3D models have been developed to simulate radiation and ecological processes for heterogeneous canopies including

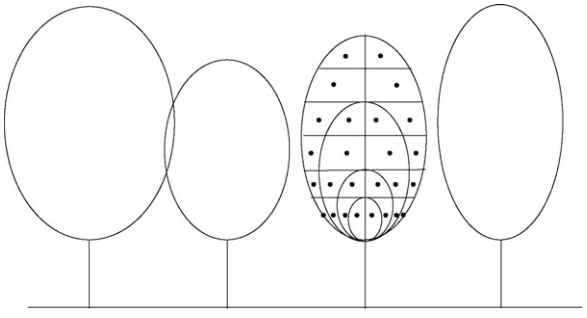

Fig. 5 – Representation of the canopy in MAESTRA. Positions and dimensions of each crown are specified. Grid volumes within the target crown are used for crown photosynthesis calculations (from Medlyn, 2004).

crops (Allen, 1974; Myneni et al., 1986a,b), orchards (Charles-Edwards and Thorpe, 1976), and forests (Wang and Jarvis, 1990; Asrar et al., 1992; Kucharik et al., 1999; Mariscal et al., 2004). The most distinguishing feature of MAESTRA is its flexibility of representing canopy with diverse types of discrete geometric envelopes (like cone, box, ellipsoid, etc.) (Fig. 5), which makes it ideal to explore the interactions between canopy structure and processes in our study.

MAESTRA is a model updated and renamed from MAESTRO (Wang and Jarvis, 1990). It incorporates the three-dimensional radiative transfer model of Norman and Welles (1983) for direct light transfer and the methods of Norman and Jarvis (1975) and Norman (1979) for diffuse light transfer. In MAESTRA, the net CO_2 assimilation rate A_n is calculated using Farquhar's model (Farquhar et al., 1980):

$$A_n = \min\{A_v, A_j\} - R_d, \tag{28}$$

$$A_v = V_{c\,max}\frac{c_i - \Gamma^*}{c_i + K_c(1 + o_i/K_o)}, \tag{29}$$

$$A_j = \frac{J}{4}\frac{c_i - \Gamma^*}{c_i + 2\Gamma^*}, \tag{30}$$

where A_v and A_j are the assimilation rate limited by Rubisco activity and electron transport (ribulose-1,5-bisphosphate, RuBP, regeneration), respectively, and R_d is the day respiration (mitochondrial respiration under illumination condition), which is the respiration from processes other than photorespiration, $V_{c\,max}$ is the maximum catalytic activity of Rubisco in the presence of saturating levels of RuBP and CO_2, c_i and o_i are the CO_2 and oxygen concentrations in the intercellular space, respectively, Γ^* is the CO_2 compensation point in the absence of day respiration and is equal to $0.5o_i/\tau$ (τ is the Rubisco specificity factor); K_c and K_o are Michaelis–Menten coefficients for CO_2 and O_2, respectively, and J is the potential rate of electron transport for a given incident photosynthetically active photon flux density I.

We calculate the potential rate of electron transport J in Eq. (30) using the following equation:

$$J = \frac{\alpha I}{\sqrt{1 + (\alpha I/J_{max})^2}}, \tag{31}$$

where J_{max} is the maximum potential rate of electron transport, α is the quantum yield (mol electron per mol photon).

The Ball–Berry stomatal conductance model (Ball et al., 1987; Collatz et al., 1992) is coupled with the photosynthesis model and leaf energy balance model to solve the net assimilation, stomatal conductance, and intercellular CO_2 mol fraction c_i, iteratively.

$$g_{sc} = a_0 + \frac{a_1 A_n h_s}{c_s} \tag{32}$$

$$A_n = g_{sc}(c_s - c_i) = g_{bc}(c_a - c_s), \tag{33}$$

where g_{sc} and g_{bc} are the stomatal and boundary layer conductances for CO_2, c_s and c_a are the CO_2 concentrations at the leaf surface and in the free air, respectively, h_s is the relative humidity at the leaf surface, a_0 and a_1 are the empirical constants.

4. Modeling radiation and photosynthesis of a savanna ecosystem

4.1. Study site

The study site is an open blue oak (*Quercus douglasii*) savanna woodland, located near Ione, California (latitude: 38.26′N, longitude: 120.57′W). The site is also part of the AmeriFlux network of eddy covariance field sites. The landscape is characterized by flat terrain (with an average slope of 1.5°) with a scattered, clumped distribution of blue oaks (*Quercus douglasii*) and a minority of grey pines (*Pinus sabiniana*) over a continuous layer of Mediterranean annual grasses. The mean annual air temperature of the region is 16.6 °C. The mean annual precipitation is about 559 mm per year (based on the data from the cooperative weather station in Ione, CA that operated between 1959 and 1977). Due to the Mediterranean climate of the region, rainfall is concentrated between October and May; essentially no rain occurs during the summer months (from June to September). The soil is classified as an Auburn very rocky silt loam (lithic haploxerepts). It contains 43% sand, 43% silt, and 13% clay. Its bulk density at surface layer (0–30 cm) is around 1.61 ± 0.10 g cm^3 ($n = 54$) (Baldocchi et al., 2004). There are two eddy covariance systems, one at 23 m and the other at 2 m above the ground, to measure the CO_2, water, energy fluxes simultaneously. A large number of meteorological variables are also measured in the site, including solar radiation, PAR, air temperature, relative

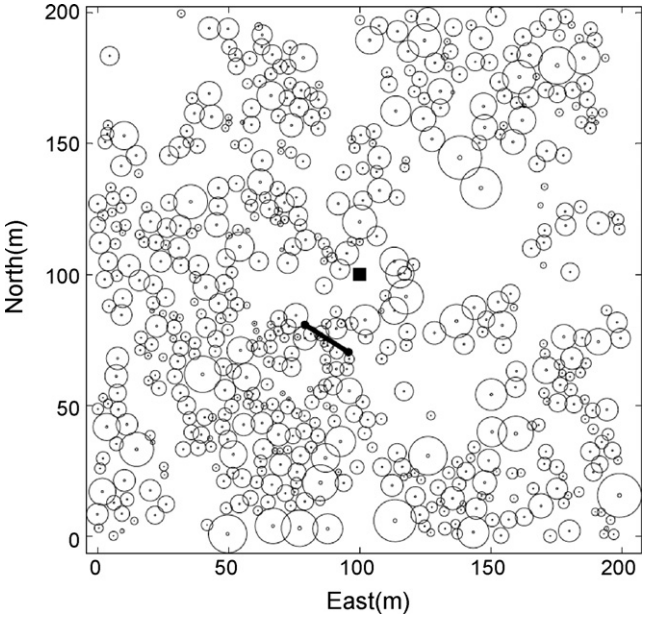

Fig. 6 – Individual trees map for 200 m by 200 m around the tower. The square dot indicates the location of the tower. And the line indicates the railtrack.

Please cite this article in press as: Chen, Q. et al., Modeling radiation and photosynthesis of a heterogeneous savanna woodland landscape with a hierarchy of model complexities, Agric. Forest Meteorol. (2008), doi:10.1016/j.agrformet.2008.01.020

Table 3 – Canopy attributes for an area of 200 m by 200 m around the tower

Variable	Value (unit)*
Tree number	576
Tree height	9.0 ± 2.7 (m)
Trunk height	1.9 ± 1.2 (m)
DBH	26 ± 11 (cm)
Crown radius	2.9 ± 1.4 (m)
Leaf area index	0.43 (m^2/m^2)
Canopy cover	0.47

* The values after the sign ± are the standard deviation.

humidity, volumetric soil moisture content, wind velocity, etc. (Baldocchi et al., 2004). Our study area covers 200 m by 200 m around the tower (Fig. 6).

4.2. *Parameterization of the model*

4.2.1. *Canopy structure*

We used airborne lidar data to map the individual-tree locations, delineate their boundaries, and extract the individual-tree structural information such as basal area, biomass, and leaf area (Chen et al., 2006, 2007a,b; Chen, 2007). The statistics of canopy structure attributes derived from lidar data are listed in Table 3. As introduced earlier, we constructed the canopy with three different settings: (1) the tree height, crown radius, trunk height, and leaf area for all trees within 200 m by 200 m are specified with the information derived from lidar data. All trees are assumed to have ellipsoidal shapes and leaves are assumed to be randomly distributed within individual crowns, (2) the canopy is simplified as a 200 m by 200 m box. The mean tree height and trunk height are used to specify the dimensions of the box. The leaf area of the box is the total leaf area over the study area. Leaves are randomly distributed within the box, and (3) the same as (2), except that the leaves are clumped and the clumping factor is calculated with our approach. We will refer the models with these three different canopy structures as individual-tree model (MAESTRA), volume integrated Poisson model (called Poisson model hereinafter), and volume integrated Markov model (called Markov model hereinafter), respectively. To avoid the edge effects, we replicate the canopy for 9 times and arrange them as a 3 by 3 grid so that the landscape is 600 m by 600 m. The simulation is only performed for 200 m by 200 m in the middle of the landscape.

4.2.2. *Spectral properties*

We measured the leaf and soil reflectance with an ASD Fieldspec FR spectroradiometer (Analytical Spectral Devices, Boulder, CO), connected to a LI-COR integrating sphere (LI-COR Inc., Lincoln, NE) for leaf reflectance measurements. The ASD Fieldspec FR spectroradiometer records the reflectance from 350 to 2500 nm in 1-nm increments. For leaves, the reflectance is 0.08 and 0.52 for the PAR and NIR wavelengths, respectively. For soil, the reflectance is 0.1 and 0.25 for the PAR and NIR wavelengths, respectively. Other spectral properties are from the literature: the transmissivity of leaves is 0.1 and 0.4 for the PAR and NIR wavelengths; the soil reflectance and leaf transmissivity at the thermal wavelength is 0.1 and 0.05, respectively (Goudriaan, 1977).

Table 4 – Physiological and other parameters

Parameter	Description	Value (unit)	Source
Photosynthesis and respiration			
α	Quantum yield	0.24 mol electron mol^{-1} photon	XB2003
K_c	Michaelis–Menten constant for CO_2 (25 °C)	275 μmol mol^{-1}	H1992
K_o	Michaelis–Menten constant for O_2 (25 °C)	420 mmol mol^{-1}	H1992
τ	Rubisco specificity factor	2321	H1992
Activation energy for temperature dependency			
ΔH_a (K_c)		79.43 kJ mol^{-1}	B2001
ΔH_a (K_o)		36.38 kJ mol^{-1}	B2001
ΔH_a (τ)		−29.0 kJ mol^{-1}	B2001
ΔH_a (R_d)		46.39 kJ mol^{-1}	B2001
ΔH_a ($V_{c\,max}$)		65.33 kJ mol^{-1}	B2001
ΔH_a (J_{max})		79.5 kJ mol^{-1}	H1992
Deactivation energy for temperature dependency			
ΔH_d ($V_{c\,max}$)		202.9 kJ mol^{-1}	H1992
ΔH_d (J_{max})		201.0 kJ mol^{-1}	H1992
Entropy term for temperature dependency			
ΔS ($V_{c\,max}$)		0.65 kJ K^{-1} mol^{-1}	H1992
ΔS (J_{max})		0.65 kJ K^{-1} mol^{-1}	H1992
Stomatal conductance			
a_0	Intercept for Ball–Berry model	0.006 mol m^{-2} s^{-1}	XB 2003
a_1	Slope for Ball–Berry model	8.88	XB 2003
Other			
	Average leaf size	0.025 m	

Note: XB 2003 (Xu and Baldocchi, 2003); B2001 (Bernacchi et al., 2001); H1992 (Harley et al., 1992).

Please cite this article in press as: Chen, Q. et al., Modeling radiation and photosynthesis of a heterogeneous savanna woodland landscape with a hierarchy of model complexities, Agric. Forest Meteorol. (2008), doi:10.1016/j.agrformet.2008.01.020

4.2.3. *Photosynthesis, respiration, and stomatal conductance*

The photosynthetic capacity $V_{c\,max}$, maximum rate of electron transport J_{max}, and day respiration R_d of blue oak leaves were measured during the growing season in 2001 by Xu and Baldocchi (2003). They conducted gas exchange measurements of CO_2 and light response curves on blue oak leaves biweekly throughout the growing season with a portable photosynthesis system (LI-6400, Li-Cor, Lincoln, NE). It was found that there are pronounced seasonal patterns of $V_{c\,max}$, J_{max}, and R_d; however, the slope for the Bell–Berry stomatal model is quite stable. The values of $V_{c\,max}$, J_{max} and R_d are normalized to 25 °C according to Eqs. (8) and (9) of Harley et al. (1992), and the temperature coefficients were from Bernacchi et al. (2001). A complete list of model parameters and the derived physiological parameters are listed in Table 4.

4.3. *Model testing*

4.3.1. *Radiation*

A 20 m railtrack was built to measure the radiation under canopy (Fig. 6). The railtrack is 1.2 m above ground and supported by tripods. A robotic tramcar, equipped with radiation sensors, moves back and forth from one end of the railtrack to the other, which typically takes 24 min for a round trip. There are three radiation sensors, including two PAR sensors for measuring downward PAR and upward PAR,

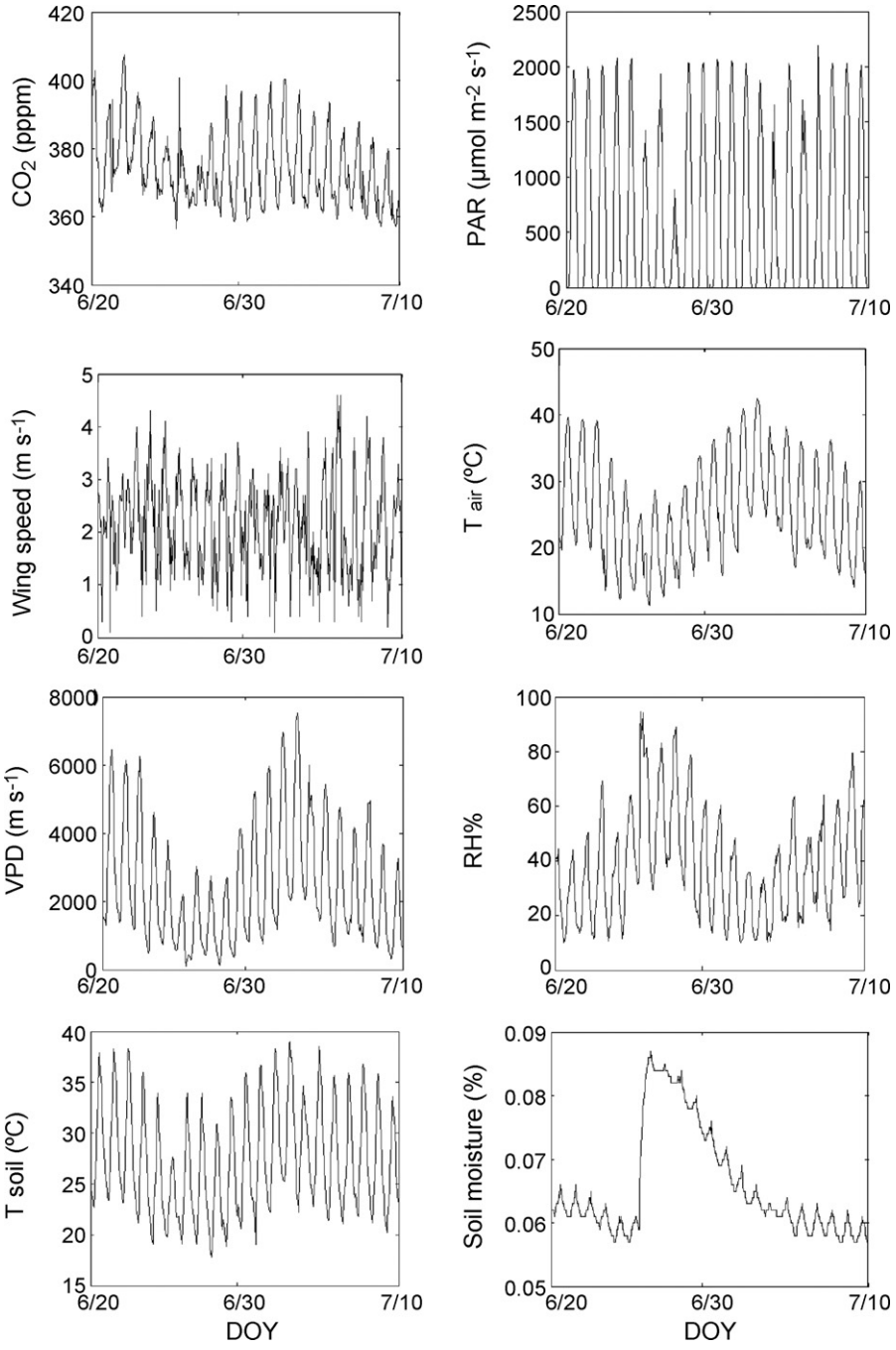

Fig. 7 – Meteorological data measured in the site.

Please cite this article in press as: Chen, Q. et al., Modeling radiation and photosynthesis of a heterogeneous savanna woodland landscape with a hierarchy of model complexities, Agric. Forest Meteorol. (2008), doi:10.1016/j.agrformet.2008.01.020

respectively, and one net radiometer sensor. The radiation measurement can be collected with 1 Hz frequency, but for most of time only the half-hour average values were recorded in a computer. Only on September 23, 2006 were measurements with 1 Hz frequency also continuously recorded from 9:30 to 14:30. The data collected during this period are used to test the model.

We run the three models (individual-tree, Poisson, and Markov models) and simulate the hourly gap fraction from 10 to 14 o'clock at 21 nodes, which divide the railtrack into 20 one-meter segments. To match the spatial domain of the gap fraction measurements by the tramcar, we only consider the trees within a rectangular area where the trees are potentially intercepting the direct sunlight to the tramcar. Therefore, the size of the rectangle varies with the solar zenith angle. Based on the field measurements, the gap fraction is computed as the ratio of the downward PAR measured by the sensor on the tramcar and the above-canopy PAR measured by the sensor on the tall tower. Within an hour, the robotic train has run for about 2.5 round trips. The average values of gap fraction derived from the sensor measurements within each hour is used to test the gap fraction simulated by the models.

4.3.2. *Photosynthesis*

We calculated the net ecosystem carbon exchange (NEE) with in-house software by processing the measurements into flux densities, correcting the canopy CO_2 storage, and filling in the missing data (Ma et al., 2007). Ecosystem respiration was estimated based on the statistical relationships between nighttime NEE and soil temperature at 4 cm depth for measurements with friction velocity greater than 0.1 m s^{-1}. Canopy photosynthesis is the difference between NEE and ecosystem respiration.

Photosynthesis is modeled for the period between June 20 and July 10 in 2001 because (1) 2001 is the year when the leaf physiological data ($V_{c\,max}$, J_{max}, and R_d) were collected, (2) in summer leaves were still active in photosynthesis while the understory grass were dead so that trees were the only biota for photosynthesis, and (3) there was a slight amount of rainfall within this period so that there is larger variation of fluxes (Fig. 7). This period also covers the longest continuous block of data with minimum missing values in 2001.

5. Results and discussion

5.1. *Comparison with field measurements*

Fig. 8 shows the hourly gap fraction derived from field measurements, individual-tree model, Poisson model, and Markov model from 10:00 to 14:00 on September 23, 2006. The values are 0.36, 0.35, 0.34, and 0.36 for tramcar measurements, individual-tree model, Poisson model, and Markov model, respectively. The gap fractions simulated by the models are close to the tramcar measurements. The difference of gap fraction among the three models is also small, especially for the latter 3 h.

Fig. 9 shows the comparison between the photosynthesis derived from the eddy covariance measurements and the ones

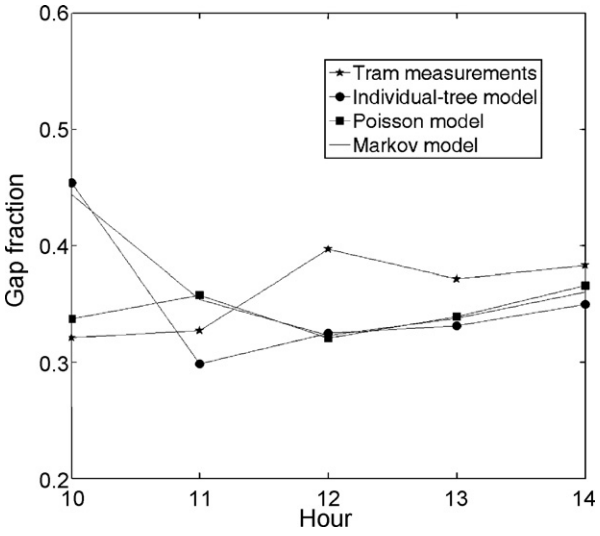

Fig. 8 – Comparison of hourly gap fraction between model simulation and tram measurements for the period of 10:00 to 14:00 on September 23, 2006.

simulated with the three models. Note that now we are considering all the trees within the 200 m by 200 m area, which is the approximate footprint size of the eddy covariance flux measurements. During the daytime, the mean photosynthesis derived from the flux measurement was -2.04 ± 3.49 μmol m^{-2} s^{-1}. The photosynthesis from the individual-tree model (filled circles with line) was -2.68 ± 1.42 μmol m^{-2} s^{-1}, which overestimate the flux measurements by 31%. The Poisson and Markov model produced flux density of $-2.71(\pm 1.46)$ and $-2.70(\pm 1.43)$ μmol m^{-2} s^{-1}, respectively. There is almost no difference between the fluxes estimations from these three models. Compared to the individual-tree based model, the mean square errors of both the Poisson models and the Markov models are negligible (about 0.005 μmol m^{-2} s^{-1}).

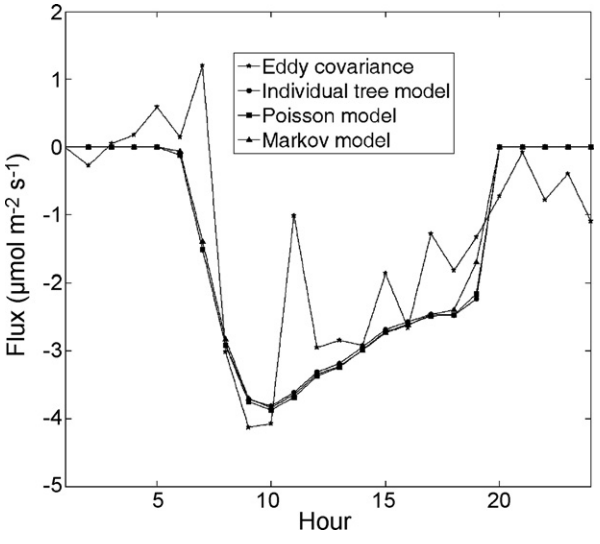

Fig. 9 – Comparison of diurnal variation photosynthesis between model simulation and eddy covariance measurements for the period of June 20 to July 10, 2001.

It seems that the three models have similar performance in modeling radiation and photosynthesis for our study site, which can be explained as follows: the simulation presented earlier (Fig. 4h) shows that when the clumping factor has a negative relationship with local leaf area index and is close to 1 when local leaf area index is small. The small local leaf area of the whole study site, which is around 0.91 m^2/m^2 (see Table 3), leads to clumping factors as large as 0.82–0.84 for the period of simulating radiation and 0.82–0.88 for the period of simulating photosynthesis. A large clumping factor

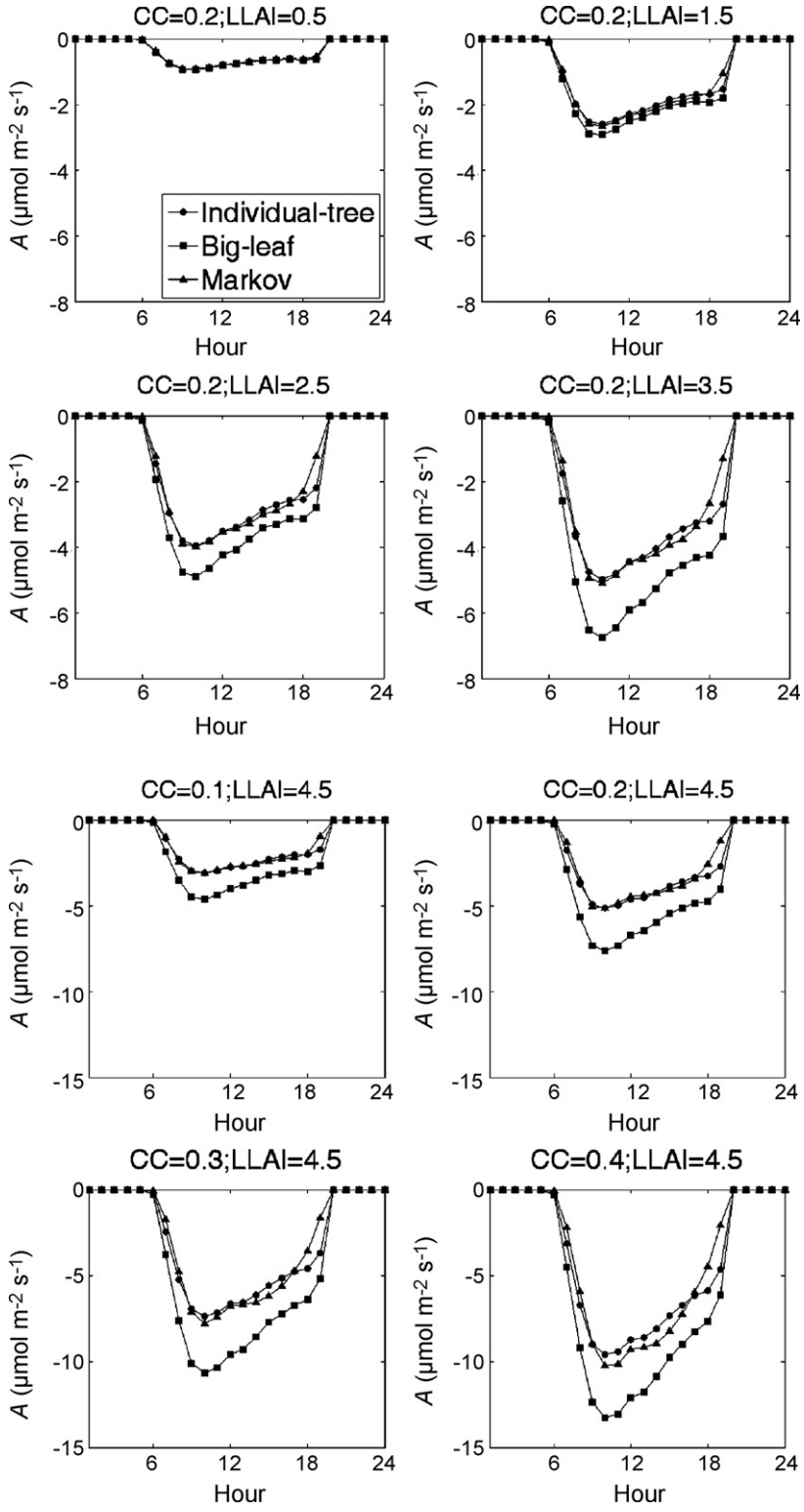

Fig. 10 – Comparison of the individual-tree based, the volume-integrated Poisson, and the volume-integrated Markov models for modeling diurnal variation of canopy CO_2 assimilation (A). CC stands for canopy cover (CC) and LLAI stands for local leaf area index.

Please cite this article in press as: Chen, Q. et al., Modeling radiation and photosynthesis of a heterogeneous savanna woodland landscape with a hierarchy of model complexities, Agric. Forest Meteorol. (2008), doi:10.1016/j.agrformet.2008.01.020

implies that there is smaller difference among these three models.

5.2. Model comparison for different canopies

Since there is almost no difference among these three models for modeling photosynthesis, we try to examine how they differ for different canopies, especially with different canopy covers and leaf area index. The canopy cover of the site is 0.47. First of all, we randomly remove a certain number of trees so that the canopy cover varies from 0.4, 0.3, 0.2, to 0.1. For each canopy cover, we multiplied the leaf areas of each tree with a certain constant so that local LAI changes from 0.5, 1, 1.5, 2, 2.5, 3, 3.5, 4, to 4.5, where local LAI is the leaf area index for canopy only. Therefore, there are a total of 36 different settings for the landscape. For each setting, we run the individual-tree, Poisson, and Markov models. The modeled canopy CO_2 assimilation is shown in Fig. 10.

The results show that (1) the Markov model produces a much better estimation of assimilation than the Poisson model when compared to the individual-tree model, and (2) the Poisson model constantly overestimates assimilation when compared to the individual-tree model. The overestimation of CO_2 assimilation by the Poisson model agrees well with the findings from previous studies because the Poisson model with no clumping will overestimate the light interception (Norman and Welles, 1983; Asrar et al., 1992; Andrieu and Sinoquet, 1993). It is very encouraging that the Markov model has a close match with the individual-tree model. The discrepancy between the Markov model and the individual-tree model could be caused by a number of factors. For example, when we derive the clumping factor, we assume the trees are regularly distributed; however, the trees in a landscape might be clumped or patched. Also, the trees are assumed to be boxes instead of ellipsoids used in the individual-tree model.

To investigate the effects of canopy cover and local leaf area index on modeling errors, we calculate the root mean square root errors of the daytime assimilation fluxes for both the Poisson model and Markov model by assuming the individual-tree model to be the truth. We also calculate the percent error, which is the ratio between the mean square root error and mean flux density of the individual-tree model. The percent error increases with the local LAI for both the Poisson and Markov models (Fig. 11).

When local LAI is as small as 0.5 m^2/m^2, the errors for both models are very small. This means that there is not much difference between the individual-tree model, Poisson, and Markov for CO_2 assimilation estimation if LAI is small. For the Poisson model, the percent error could be as high as nearly 50% when local leaf area index is 4.5; however, the maximum percent error for the Markov model is only about 10%.

The Poisson model and Markov model show different patterns of errors depending on canopy cover. For the Poisson model, the errors decrease with canopy cover. This is reasonable because canopy is more like a big-leaf as canopy cover increases. However, for the Markov model, the errors increase with canopy cover. This can be explained by the approach of calculating clumping factors. Larger canopy cover implies smaller tree spacing. Our analysis in the next section

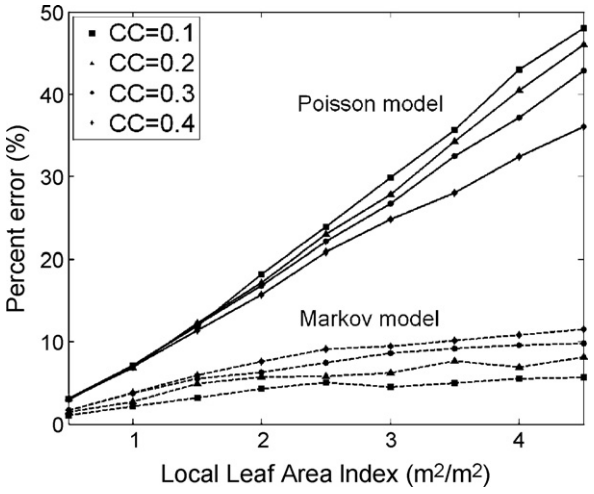

Fig. 11 – The dependence of percent errors of the integrated-volume Poisson model (solid lines) and the integrated-volume Markov model (dashed lines) on canopy cover and local LAI. The errors are calculated based on the daytime assimilation fluxes assuming the flux from the individual-tree model to be the truth.

shows that the clumping factor is more sensitive to tree spacing when trees are close to each other. So, a small error in setting the tree spacing could cause a large variation of clumping factor, therefore, a larger error in carbon flux estimation.

5.3. Dependence of clumping factor on solar zenith angle

Although more theoretical insights are needed to examine the direction dependence of clumping (Weiss et al., 2004), only a few studies have addressed this issue (Andrieu and Sinoquet, 1993; Kucharik et al., 1999). Kucharik et al. (1999) used MVI (Multiband Vegetation Imager) or TRACs (Tracing Radiation and Architecture of Canopies) measurements to derive the element clumping index that quantifies the effect of foliage

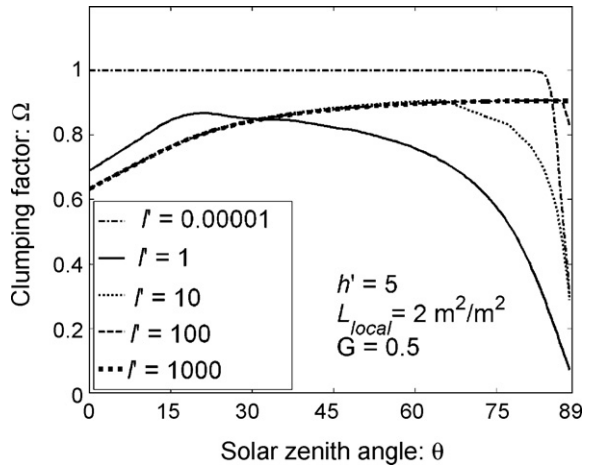

Fig. 12 – The dependence of clumping factors on solar zenith angle for canopies with different tree spacing to crown width ratio (l′).

clumping at scales larger than individual leaves or shoots. For five forest species (jack pine, black spruce, aspen, oak, and sugar maple), they found that the element clumping index generally increases with solar zenith angle, which shows different patterns as simulated in Fig. 4(j).

To examine the directional dependence of clumping in more details, we calculated clumping factors by setting the tree spacing to crown width ratio (l') at five different values (0.00001, 1, 10, 100, 1000) with the solar zenith angle θ varying from 0 to 89° (Fig. 12). A small l' of 0.00001 corresponds to an approximately continuous canopy, in which case the clumping factors are supposed to be 1 for different solar zenith angles. The results confirm such a pattern except when θ is greater than 84° (Fig. 12). When θ is as large as 84° and l' is as small as 0.00001, a' has a small value of about 10^{-6} and the corresponding subvolume is very small too (Fig. 2). In such a situation, the computation will produce numerical overflow errors because we use a numerical method called Gaussian quadrature to calculate the integral in Eq. (23).

However, for other four l' values, even the smallest a' is 0.0175, which is much larger than 10^{-6}. Therefore, it is unlikely that the decrease of Ω is also caused by the numerical errors for these l' values. When l' is equal to 10 or 100, Ω increases with θ at the very beginning and then decreases at 63.4° or 87.1°, respectively. These two angles correspond to the angles at which neighboring trees are starting to block each other. Sunlight interception by neighboring trees leads to smaller sunlit leaf area index and thus smaller clumping factors. When l' is equal to 1000, trees do not shade each other even when θ is at the maximum angle of 89° so the clumping factor keeps increasing. These different patterns indicate that clumping factors increase with solar zenith angle only in certain conditions.

Besides l', our simulations (results not shown) indicate that the angular dependence of clumping factors is also related to the other three parameters (tree height to crown width ratio h', local leaf area index L_{local}, and G-function value). Unlike the empirical approach used in Kucharik et al. (1999), our analytical approach allow us to examine the relationship between clumping factors and solar zenith angle by just changing the input parameters and without being limited by the field data.

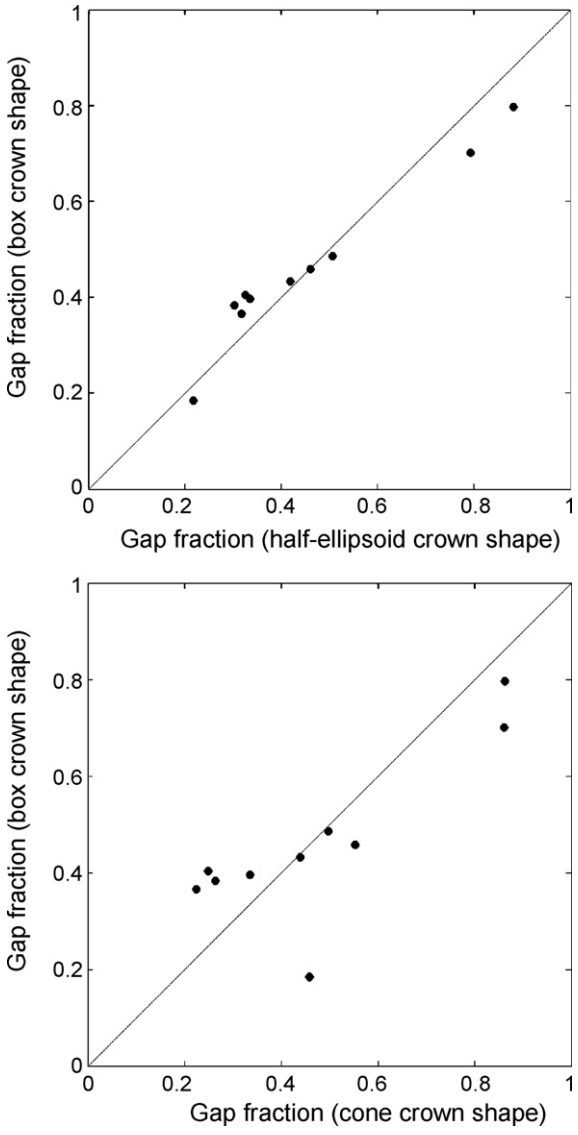

Fig. 13 – Comparison of gap fractions simulated by MAESTRA with different crown shapes for trees around the railtrack from 8 a.m. to 5 p.m. on September 23, 2006. (Upper) box vs. half-ellipsoidal shapes; (lower) box vs. cone shapes.

5.4. *Further research*

Despite of the usefulness of our method of calculating clumping factors has been demonstrated by comparing the results from the Markov model with tower CO_2 flux measurements and the results from more complex 3D individual-tree based model, more research need to be done in the following aspects.

First of all, the current approach of calculating clumping factors is based on the assumption that each tree has a box shape. Box shape might be a reasonable approximation of deciduous trees. However, for other vegetation types such as conifers, such an assumption might be questionable. As a preliminary study to examine the effects of canopy shape, we modeled the trees around the trailtrack with three different shapes (half-ellipsoid, box, and cone) and compared the simulated hourly gap fractions from 8 a.m. to 5 p.m. on September 23, 2006 (Fig. 13). It was found that the mean gap fractions are 0.456, 0.460, and 0.475 when the individual-tree shapes are half-ellipsoid, box, and cone, respectively. The gap fractions between box and half-ellipsoid shapes have only 1% difference. The difference between box and cone shapes increases to 3%. Therefore, it would be better if we can develop analytical approach to calculate clumping factors for conifer forest with cone shapes to further reduce the errors.

Second, we only consider the crown-level clumping, which means at the landscape level the leaves are organized into individual crown envelopes (or clumps) and within each crown envelope leaves are randomly distributed. However, clumping could exist at different levels including shoot, branch, whorl, and crown levels (Bréda, 2003; Walter et al., 2003). The clumping at the shoot, branch, and whorl levels

Please cite this article in press as: Chen, Q. et al., Modeling radiation and photosynthesis of a heterogeneous savanna woodland landscape with a hierarchy of model complexities, Agric. Forest Meteorol. (2008), doi:10.1016/j.agrformet.2008.01.020

could play an important role in the whole canopy clumping, which is especially true for conifers (Chen, 1996). Although in a very open deciduous savanna woodland, crown clumping could be the dominant clumping factor due to the large open space, more research need to be done in the future to consider the within-crown clumping.

Third, the current approach is tested over a relatively small area (200 m by 200 m). Further research is needed to explore on how to calculate clumping factor for larger spatial scales, especially in the scale of grid size for numerical weather prediction (NWP) and general circulation models (GCM), which is typically 10–100 km. At such a large spatial scale, the landscape typically consists of large patches of different land use and land cover types (water, soil, forest land, wheat fields, etc.). How to calculate the clumping factor at different spatial scale (especially the broad spatial scale) deserves more research.

Last but not the least, the calculation of clumping factors with the *normalized* equations requires a total of five input parameters, two of which are challenging to obtain at the large spatial scale: crown depth to crown width ratio and tree spacing to crown width ratio. The computation of these parameters requires high-spatial resolution remotely sensed data. Airborne lidar data are particularly suitable for calculating the canopy height, tree size, and tree spacing. High-spatial resolution imagery such as IKONOS and QuickBird can also provide information about tree size and tree spacing. In the future, it is necessary to investigate how to extract these parameters with remotely sensed data at the large spatial scales.

6. Conclusions

This study presents an analytical approach to calculate clumping factors for heterogeneous landscapes and uses it in the Markov model for modeling CO_2 assimilation of canopy. It was found that the CO_2 assimilation estimated by the Markov model can closely match the one by the individual-tree based model for landscapes with different canopy cover and local leaf area index. It is expected that our approach can significantly improve our ability of predicting ecosystem functions for heterogeneous landscapes from regional to global scales. Research is needed to explore how to estimate the input parameters at the broader spatial scales with remote sensing technologies such as LIDAR and MISR (Multiangle Imaging SpectroRadiometer).

Acknowledgements

Great thanks are given to Belinda Medlyn and Yingping Wang for their explanation in using MAESTRA. We also acknowledge Liukang Xu, Siyan Ma, Youngryel Ryu, and Ted Hehn for their help in collecting data for our model parameterization and validation. The robotic tramcar system was designed by Ted Hehn. Qi Chen is thankful for the funding support from the NASA Earth System Science Fellowship. This research was supported in part by the Office of Science (BER), U.S. Department of Energy, Grant No. DE-FG02-03ER63638 and through the Western Regional Center of the National Institute for Global Environmental Change under Cooperative Agreement No. DE-FC02-03ER63613. Great thanks are also extended to Dr. John Gash and two anonymous reviewers for their constructive suggestions and comments on the manuscript. The code for computing clumping factors is available from the senior-author upon request.

REFERENCES

Allen, L.H., 1974. A model of light penetration in a wide row crop. Agronomy J. 66, 41–47.
Andrieu, B., Sinoquet, H., 1993. Evaluation of structure description requirements for predicting gap fraction of vegetation canopies. Agric. Forest Meteorol. 65, 202–227.
Asrar, G., Myneni, R.B., Choudhury, B.J., 1992. Spatial heterogeneity in vegetation canopies and absorbed photosynthetically active radiation: a modeling study. Remote Sens. Environ. 41, 85–103.
Baldocchi, D.D., Harley, P.C., 1995. Scaling carbon dioxide and water vapor exchange from leaf to canopy in a deciduous forest: model testing and application. Plant, Cell Environ. 18, 1157–1173.
Baldocchi, D.D., Hutchison, B.A., Matt, D.R., McMillen, R.T., 1985. Canopy radiative transfer models for spherical and known leaf inclination distribution angles: a test in an oak-hickory forest. J. Appl. Ecol. 22, 539–555.
Baldocchi, D.D., Fuentes, J., Bowling, D., Turnipseed, A., Monson, R., 1999. Scaling isoprene fluxes from leaves to canopies: test cases over a boreal aspen and a mixed temperate forest. J. Appl. Meteorol. 38, 885–898.
Baldocchi, D.D., Xu, L., Kiang, N., 2004. How plant functional-type, weather, seasonal drought, and soil physical properties alter water and energy fluxes of an oak-savanna and an annual grassland. Agric. Forest Meteorol. 123, 13–39.
Ball, J.T., Woodrow, I.E., Berry, J.A., 1987. A model predicting stomatal conductance and its contribution to the control of photosynthesis under different environmental conditions. In: Biggins, J. (Ed.), Progress in Photosynthesis Research, vol. 4. M Nijhoff, Dordrecht, pp. 221–224.
Bernacchi, C.J., Singsaas, E.L., Pimentel, C., Portis, A.R., Long, S.P., 2001. Improved temperature response functions for models of Rubisco-limited photosynthesis. Plant, Cell Environ. 24, 253–260.
Bond, W.J., Midgley, G.F., Woodward, F.I., 2003. The importance of low atmospheric CO_2 and fire in promoting the spread of grasslands and savannas. Global Change Biol. 9, 973–982.
Bréda, N., 2003. Ground-based measurements of leaf area index: a review of methods, instruments and current controversies. J. Exp. Bot. 54, 2403–2417.
Charles-Edwards, D.A., Thorpe, M.R., 1976. Interception of diffuse and direct beam radiation by a hedgerrow apple orchard. Ann. Bot. 40, 603–613.
Chen, J.M., 1996. Optically-based methods for measuring seasonal variation of leaf area index in boreal conifer stands. Agric. Forest Meteorol. 80, 135–163.
Chen, Q., 2007. Airborne lidar data processing and information extraction. Photogrammetric Eng. Remote Sens. 73, 109–112.
Chen, Q., Gong, P., 2004. Automatic variogram parameter extraction for textural classification of high resolution IKONOS imagery. IEEE Trans. Geosci. Remote Sens. 42, 1106–1115.
Chen, J.M., Menges, C.H., Leblanc, S.G., 2005. Global derivation of the vegetation clumping index from multi-angular satellite data. Remote Sens. Environ. 97, 447–457.

Chen, Q., Baldocchi, D.D., Gong, P., Kelly, M., 2006. Isolating individual trees in a savanna woodland using small footprint LIDAR data. Photogrammetric Eng. Remote Sens. 72, 923–932.

Chen, Q., Gong, P., Baldocchi, D.D., Xie, G., 2007a. Filtering airborne laser scanning data with morphological methods. Photogrammetric Eng. Remote Sens. 73, 175–185.

Chen, Q., Gong, P., Baldocchi, D.D., Tian, Y.Q., 2007b. Estimating basal area and stem volume for individual trees from lidar data. Photogrammetric Eng. Remote Sens. 73, 1355–1365.

Collatz, G.J., Ribas-Carbo, M., Berry, J.A., 1992. A coupled photosynthesis-stomatal conductance model for leaves of C4 plants. Aust. J. Plant Physiol. 19, 519–538.

De Wit, C.T., 1965. Photosynthesis of leaf canopies. Agric. Res. Rept., Wageningen 663, 1–57.

Farquhar, G.D., von Caemmerer, S., Berry, J.A., 1980. A biochemical model of photosynthetic CO_2 assimilation in leaves of C_3 species. Planta 149, 78–90.

Goudriaan, J., 1977. Crop micrometeorology: a simulation study. In: Simulation Monographs, Pudoc, Wageningen (Netherlands), 257 pp.

Gower, S.T., Kucharik, C.J., Norman, J.M., 1999. Direct and indirect estimation of leaf area index, fAPAR and net primary production of terrestrial ecosystems. Remote Sens. Environ. 70, 29–51.

Harley, P.C., Thomas, R.B., Reynolds, J.F., Strain, B.R., 1992. Modelling photosynthesis of cotton grown in elevated CO_2. Plant, Cell Environ. 15, 271–282.

Jarvis, P.G., Leverenz, J.W., 1983. Productivity of temperate, deciduous and evergreen forests. In: Lange, O.L., Nobel , P.S., Osmond, C.B., Ziegler, H. (Eds.), Encyclopedia of Plant Physiology, 12D Physiological Plant Ecology IV. Ecosystem Processes: Mineral Cycling, Productivity and Man's Influence. Springer–Verlag, Berlin, pp. 234–280.

Jonckheere, I., Fleck, S., Nackaerts, K., Muys, B., Coppin, P., Weiss, M., Baret, F., 2004. Methods for leaf area index determination. Part I: theories, techniques and instruments. Agric. Forest Meteorol. 121, 19–35.

Jonckheere, I., Nackaerts, K., Muys, B., van Aardt, J., Coppin, P., 2006. A fractal dimension-based modelling approach for studying the effect of leaf distribution on LAI retrieval in forest canopies. Ecol. Model. 197 (1–2), 179–195.

Kucharik, C.J., Norman, J.M., Gower, S.T., 1999. Characterization of the radiation regimes in nonrandom forest canopies: theory, measurements, and a simplified modeling approach. Tree Physiol. 19, 695–706.

Ma, S., Baldocchi, D.D., Xu, L., Hehn, T., 2007. Interannual variability in carbon exchange of an oak/grass savanna and an annual grassland in California. Agric. For. Meteorol. 147, 157–171.

Mariscal, M.J., Martens, S.N., Ustin, S.L., Chen, J., Weiss, S.B., Roberts, D.A., 2004. Light transmission profiles in an old-growth forest canopy: simulations of photosynthetically active radiation by using spatially explicit radiative transfer models. Ecosystems 7, 454–467.

Medlyn, B.E., 2004. A MAESTRO retrospective. In: Mencuccini, M., Grace, J.C., Moncrieff, J., McNaughton, K. (Eds.), Forests at the Land–Atmosphere Interface. CAB International, pp. 105–121.

Monteith, J.L., 1965. Light distribution and photosynthesis in field crops. Ann. Bot. 29, 17–37.

Myneni, R.B., Asrar, G., Kanemasu, E.T., Lawlor, D.J., Impens, I., 1986a. Canopy architecture, irradiance distribution in leaf surfaces and consequent photosynthetic efficiencies in heterogeneous plant canopies. Part I. Theoretical considerations. Agric. Forest Meteorol. 37, 189–204.

Myneni, R.B., Asrar, G., Kanemasu, E.T., Lawlor, D.J., Impens, I., 1986b. Canopy architecture, irradiance distribution in leaf surfaces and consequent photosynthetic efficiencies in heterogeneous plant canopies. Part II. Results and discussion. Agric. Forest Meteorol. 37, 205–218.

Nilson, T., 1971. A theoretical analysis of the frequency of gaps in plant stands. Agric. Meteorol. 8, 25–38.

Nilson, T., 1999. Inversion of gap frequency data in forest stands. Agric. Forest Meteorol. 98–99, 437–448.

Norman, J.M., 1979. Modeling the complete crop canopy. In: Barfield, B.J., Gerber, J.F. (Eds.), Modification of the Aerial Environment of Plants. American Society of Agricultural Engineers, Michigan, pp. 249–277.

Norman, J.M., Jarvis, P.G., 1975. Photosynthesis in Sitka spruce (*Picea sitchensis* (Bong.) Carr.) V. Radiation penetration theory and a test case. J. Appl. Ecol. 12, 839–878.

Norman, J.M., Welles, J.M., 1983. Radiative transfer in an array of canopies. Agronomy J. 75, 481–488.

Pinty, B., Gobron, N., Widlowski, J.L., Lavergne, T., Verstraete, M.M., 2004. Synergy between 1-D and 3-D radiation transfer models to retrieve vegetation canopy properties from remote sensing data. J. Geogr. Res. 109, D21205, doi:10.1029/2004JD005214.

Ramankutty, N., Foley, J.A., 1999. Estimating historical changes in global land cover: croplands from 1700 to 1992. Global Biogeochem. Cycles 13, 997–1027.

Ross, J., 1981. The Radiation Regime and Architecture of Plant Stands. Junk Publishers, The Hague, 391 pp.

Sankaran, M., Hanan, N.P., Scholes, R.J., Ratnam, J., Augustine, D.J., Cade, B.S., Gignoux, J., Higgins, S.I., Le Roux, X., Ludwig, F., Ardo, J., Banyikwa, F., Bronn, A., Bucini, G., Caylor, K.K., Coughenour, M.B., Diouf, A., Ekaya, W., Feral, C.J., February, E.C., Frost, P.G., Hiernaux, P., Hrabar, H., Metzger, K.L., Prins, H.H., Ringrose, S., Sea, W., Tews, J., Worden, J., Zambatis, N., 2005. Determinants of woody cover in African savannas: a continental scale analysis. Nature 438, 846–849.

Sellers, P.J., Randall, D.A., Collatz, C.J., Berry, J.A., Field, C.B., Dazlich, D.A., Zhang, C., Collelo, C.D., 1996. A revised land surface parameterization (SiB2) for atmospheric GCMs. Part 1: model formulation. J. Climate 9, 676–705.

Sinclair, T., Murphy, C., Knoerr, K., 1976. Development and evaluation of simplified models for simulating canopy photo synthesis and transpiration. J. Appl. Ecol. 13, 813–829.

Walter, J.N., Fournier, R.A., Soudani, K., Meyer, E., 2003. Integrating clumping effects in forest canopy structure: an assessment through hemispherical photographs. Can. J. Remote Sens. 29, 388–410.

Wang, Y.P., Jarvis, J.P., 1990. Description and validation of an array model-MAESTRO. Agric. Forest Meteorol. 51, 257–280.

Weiss, M., Baret, F., Smith, G., Jonckheere, I., Coppin, P., 2004. Review of methods for in situ leaf area index (LAI) determination: Part II. Estimation of LAI, errors and sampling. Agric. Forest Meteorol. 121, 37–53.

Xu, L., Baldocchi, D.D., 2003. Seasonal trend of photosynthetic parameters and stomatal conductance of blue oak (*Quercus douglasii*) under prolonged summer drought and high temperature. Tree Physiol. 23, 865–877.

Please cite this article in press as: Chen, Q. et al., Modeling radiation and photosynthesis of a heterogeneous savanna woodland landscape with a hierarchy of model complexities, Agric. Forest Meteorol. (2008), doi:10.1016/j.agrformet.2008.01.020